Pseudo-Contact NMR Shifts over the Paramagnetic Metalloprotein CoMMP-12 from First Principles

Pseudo-contact NMR shifts over a paramagnetic metalloprotein (CoMMP-12) from first principles

Ladislav Benda,[a,b] Jiří Mareš,[c] Enrico Ravera,[d] Giacomo Parigi,[d] Claudio Luchinat,[d] Martin Kaupp,[a],* and Juha Vaara[c],*

Dedication ((optional))

Abstract: Long-range pseudo-contact NMR shifts (PCSs) provide important restraints for the structure refinement of proteins when a paramagnetic metal center is present, either naturally or introduced artificially. Here we show that *ab initio* quantum-chemical methods and a modern version of the Kurland-McGarvey approach for paramagnetic NMR (pNMR) shifts in the presence of zero-field splitting (ZFS) together provide accurate predictions of all PCSs in a metalloprotein (high-spin cobalt-substituted MMP-12 as a test case). Computations of 314 ^{13}C PCSs via *g*- and ZFS-tensors based on multi-reference methods provide a reliable bridge between EPR-parameter- and susceptibility-based pNMR formalisms. Due to the high sensitivity of PCSs to even small structural differences, local structures based either on X-ray diffraction or on various DFT optimizations could be evaluated critically by comparing computed and experimental PCSs. Many DFT functionals provide insufficiently accurate structures. We also found the available 1RMZ PDB X-ray structure to exhibit deficiencies related to binding of a hydroxamate inhibitor. This has led to a newly refined PDB structure for MMP-12 (5LAB) that provides a more accurate coordination arrangement and PCSs.

The anisotropic magnetic susceptibility[1] of paramagnetic metal ions induces the so-called pseudo-contact shifts (PCSs) in NMR spectra, which can be observed for nuclei between 5 Å and 40 Å from the metal center.[2] PCSs provide precious structural information on the biomolecules on which they are measured, both in solution and in the solid state.[3] PCS-based structural restraints have also become important for protein NMR crystallography.[4] Their importance is further enhanced by recent developments in fast magic-angle spinning (MAS) combined with high-field instruments.[4d, 5] While PCSs can thus provide crucial information on the structure of a metalloprotein as a whole, NMR is typically blind to nuclei near the paramagnetic metal center due to fast paramagnetic relaxation. The computation of pNMR shifts by first-principles quantum-chemical (QC) methods, on the other hand, has recently progressed appreciably, in particular by inclusion of the non-contact terms in small to medium-sized molecules, with no fundamental limitations close to the metal center.[6] There has so far been no attempt to access the long-range PCSs in larger biological systems by first-principles calculations, as the molecular sizes needed for an explicit treatment of the hyperfine coupling (HFC) anisotropies appeared prohibitive.

Here we show that introduction of the point-dipole approximation (PDA), appropriate for the long-range spin-dipolar HFCs, into modern quantum-chemical pNMR shift machinery can be used to compute long-range PCSs based on accurate multi-reference *ab initio* calculations of *g*- and zero-field splitting (ZFS) *D*-tensors. Using such a combined approach, we have computed the entire set of 314 previously measured ^{13}C long-range PCSs[4a] (and further shifts from nuclei closer to the metal center[5]) in high-spin cobalt(II)-substituted human matrix metalloproteinase catalytic domain (CoMMP-12), a 17 kDa paramagnetic metalloprotein for which extensive experimental studies of structure and pNMR shifts are available.[4a, 4b, 5, 7] Not only could comparison of computed and experimental PCSs be used to critically evaluate the quality of input structures obtained from either experimental or computational sources, but the calculations also allow us to relate the long-range PCS information to the local molecular and electronic structure around the paramagnetic metal center.

Our computations are based on a modern quantum-chemical implementation[6d] of Kurland-McGarvey theory,[8] which derives the pNMR shift tensor from EPR spin Hamiltonian parameters (the *g*-, HFC-, and *D*-tensors). While the full pNMR formalism includes also the contact and Ramsey-type orbital shielding terms (see Supporting Information, SI), here we focus mainly on the dipolar shift tensor of a nucleus *K*, $\boldsymbol{\delta}_K^{\mathrm{dip}}$, which upon rotational averaging gives the PCS. The dipolar shift tensor may be identified with the terms of the pNMR shift due to the spin-dipolar part of the HFC tensor, $\mathbf{A}_K^{\mathrm{SD}}$.[6d]

$$\boldsymbol{\delta}_K^{\mathrm{dip}} = \frac{\mu_{\mathrm{B}}}{kT\hbar\gamma_K}\mathbf{g}\cdot\langle\boldsymbol{SS}\rangle\cdot\mathbf{A}_K^{\mathrm{SD}}, \qquad (1)$$

where μ_{B}, k, T, and γ_K are, respectively, the Bohr magneton, Boltzmann constant, absolute temperature, and nuclear gyromagnetic ratio in $\mathrm{rad}\cdot\mathrm{s}^{-1}\cdot\mathrm{T}^{-1}$. $\mathbf{g}$ is the *g*-tensor, and the (electron) spin dyadic $\langle\boldsymbol{SS}\rangle$ represents a thermal average of the two spin operators over the eigenstates of the ZFS Hamiltonian with the inclusion of magnetic couplings between those states (see SI for details). Without applying the PDA, a first-principles treatment not only of *g*-, *D*-, but also of $\mathbf{A}_K^{\mathrm{SD}}$ would be needed. While the *g*- and *D*-tensors are dominated by the local spin

[a] Dr. L. Benda, Prof. Dr. Martin Kaupp
Institut für Chemie, Theoretische Chemie
Technische Universität Berlin
Sekr. C7, Straße des 17. Juni 135, 10623 Berlin, Germany
E-mail: martin.kaupp@tu-berlin.de
[b] Dr. L. Benda
Institut des Sciences Analytiques
UMR 5280 CNRS / ENS Lyon / UCB Lyon 1
5 rue de la Doua, 69100 Villeurbanne, France
[c] Dr. Jiří Mareš, Prof. Dr. Juha Vaara
NMR Research Unit
University of Oulu
P.O. Box 3000, 90014 Oulu, Finland
E-mail: juha.vaara@iki.fi
[d] Dr. E. Ravera, Prof. Dr. G. Parigi, Prof. Dr. C. Luchinat
Magnetic Resonance Centre
University of Florence
Via Luigi Sacconi 6, 50019 Sesto Fiorentino, Italy

Supporting information for this article is given via a link at the end of the document.

density distribution around the metal center and are accessible from relatively small models, explicit and accurate QC computation of $\mathbf{A}_K^{\mathrm{SD}}$ would be required for all protein atoms for which PCSs are desired, currently a prohibitive task. Within the PDA, the spin-dipolar HFC is approximated as

$$\mathbf{A}_K^{\mathrm{SD}} \approx \frac{\mu_0 \mu_B g_e}{4\pi r_{IS}^3} \hbar \gamma_K \mathbf{P}_{IS}, \qquad (2)$$

where g_e is the free-electron g-value, $\mathbf{P}_{IS} = 3\mathbf{r}_{IS}\mathbf{r}_{IS}/r_{IS}^2 - \mathbf{1}$ is the dimensionless dipolar coupling tensor, $\mathbf{1}$ a 3×3 unit matrix, and $\mathbf{r}_{IS}$ is a vector connecting the positions of nuclear spin $\mathbf{I}_K$ and of electron spin $\mathbf{S}$ (see also ref. [9] for a recent use of the PDA in the context of QC PCS calculations). Within the PDA, which underlies also the usual interpretation of long-range PCS measurements,[1, 8] $\mathbf{A}_K^{\mathrm{SD}}$ is determined solely by $\mathbf{r}_{IS}$, and no QC computation of HFC tensors is required. Inserting (2) into (1) gives the expression for the dipolar shift tensor:

$$\boldsymbol{\delta}_K^{\mathrm{dip}} \approx \frac{\mu_0 \mu_B^2 g_e}{4\pi r_{IS}^3 kT} \mathbf{g} \cdot \langle \mathbf{SS} \rangle \cdot \mathbf{P}_{IS}. \qquad (3)$$

A QC treatment is now only required for the g- and D-tensor (the latter is needed to compute $\langle \mathbf{SS} \rangle$), which determine the magnetic anisotropy around the metal center. This anisotropy is often expressed via the traceless symmetric susceptibility tensor $\boldsymbol{\chi}$,[1] which relates to the dipolar shift tensor as

$$\boldsymbol{\delta}_K^{\mathrm{dip}} = \frac{\boldsymbol{\chi} \cdot \mathbf{P}_{IS}}{4\pi r_{IS}^3}. \qquad (4)$$

Comparing (3) and (4), the susceptibility tensor in the present context may be written as

$$\boldsymbol{\chi}' \approx \frac{\mu_0 \mu_B^2 g_e}{kT} \mathbf{g} \cdot \langle \mathbf{SS} \rangle. \qquad (5)$$

To be consistent with standard treatments in the literature,[1, 8] a symmetric expression involving $\mathbf{g} \cdot \langle \mathbf{SS} \rangle \cdot \mathbf{g}^T$ would be required (^{T} denoting matrix transpose). However, this would be inconsistent with the employed pNMR shift theory based on an EPR spin-Hamiltonian, developed systematically up to next-to-leading order in the fine structure constant.[6a, 6d] We will thus identify $\boldsymbol{\chi}$ with the symmetric part of $\boldsymbol{\chi}'$ (eq. (5); see SI for more details).

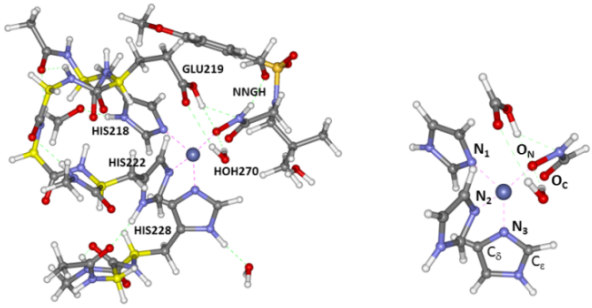

Figure 1. Models of the CoMMP-12 protein catalytic center: *m1* (left, 170 atoms; C_α atoms in light yellow) used for DFT optimizations and *m0* (right, 42 atoms) used for *ab initio* g- and D-tensor calculations, with notation of the metal-coordinating atoms: the labels N_1, N_2, N_3 correspond to HIS218, HIS222, HIS228, respectively, C_δ and $C\varepsilon$ label the histidine carbon atoms neighboring the coordinating nitrogen, and O_N and O_C are the hydroxamate oxygen atoms of the NNGH inhibitor.

This link between EPR-parameter- and susceptibility-based PCS formalisms provides the basis for our multi-scale modeling of the PCSs in the Co^{II}-substituted catalytic domain of the MMP-12 enzyme: our initial starting point for various DFT optimizations was a 170-atom model of the cobalt active site (model *m1*, Figure 1) taken from the X-ray crystal structure of the native zinc enzyme (ZnMMP-12, PDB file 1RMZ[7c]), keeping the seven C_α atoms fixed at their PDB positions. Alternatively, the coordinates of the same 170 atoms were taken directly from the 1RMZ structure (after re-optimization of just the hydrogen atom positions) and, at a later stage, from the newly refined 5LAB PDB structure (see below). Further details of the computations are provided in SI (see also Table S1).

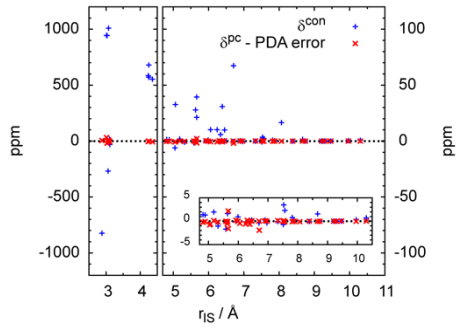

Figure 2. ^{13}C contact shifts (blue +) and PDA errors (red ×) as functions of the distance from the metal center in model *m1*. The PDA error was evaluated as the difference between the isotropic value of the full ^{13}C dipolar shift tensor according to eq. (1) and the approximate ^{13}C PCSs calculated according to eq. (3). PBE0//PBE0-D3 results for HFCs (*m1*), NEVPT2//PBE0-D3 results for g- and D-tensors (*m0*), 280 K used as temperature for shift calculations. The insert shows a blow-up of a subsection.

The validity of the PDA of eq. (3) for the PCS (δ^{pc}) and the (un-)importance of contact contributions (δ^{con}) for the long-range shifts were examined using hybrid DFT calculations for the HFC tensor and the full pNMR treatment (eq. (S4) in SI). The results are shown in Figure 2. While deviations of the PDA from the full treatment vanish already well before a distance of 7 Å from the metal center, contact contributions are relevant within the nearest covalent network of the metal ligands up to about 8 Å. Thus, for all practical purposes, whenever the contact shift can be neglected, the PDA can be safely used. As all of the 314 shifts, for which we will apply the PDA, pertain to ^{13}C nuclei beyond 8 Å, the chosen approximations are clearly adequate. Closer to the metal center, a full treatment is needed, but then the nuclei of interest are mostly contained within our *m1* model.

As we needed to compute the g- and D-tensors of this high-spin Co^{II} system at the NEVPT2(7,5) multi-reference *ab initio* level[10] (see Table S2 in SI for the insufficient accuracy of DFT methods), the computational demands of these calculations required a further truncation of our molecular models. Smaller 42-atom models *m0* were thus cut out of the various *m1* structures (Figure 1), with subsequent optimization of the terminating hydrogen-atom positions. The chosen computational level is known to provide accurate g- and D-tensors for high-spin Co^{II} complexes,[6c, 11] and we have ascertained that the size of model *m0* is adequate (Table S2).

Table 1. Comparison between calculated[a] and experimental susceptibility tensor parameters, and statistics for agreement between calculated and experimental PCSs

	1RMZ	5LAB	optimized structures						**fitted exp.**
			BP86	BP86-D3	B3LYP	BLYP35-D3	PBE0	PBE0-D3	
χ_{11} [b,c]	-6.0	-4.6	-3.2	-3.0	-4.1	-5.3	-5.2	-4.0	**-4.7**
χ_{22} [b,c]	-2.4	-1.1	0.3	0.3	0.8	-0.3	-0.1	-1.1	**-1.9**
χ_{33} [b,c]	8.3	5.7	2.9	2.6	3.2	5.6	5.2	5.2	**6.7**
$\Delta\chi_{ax}$ [c]	12.5	8.6	-4.9	-4.4	-6.1	8.4	7.9	7.7	**10.0**
$\Delta\chi_{rh}$ [c]	-3.6	-3.6	2.6	2.3	2.4	-5.0	-5.1	-2.9	**-2.8**
φ [d]	157	166	175	174	170	173	168	167	**158**
ϑ [d]	-94	-99	-128	-126	-142	-99	-112	-97	**-97**
ψ [d]	20	16	-54	-54	-21	7	7	12	**21**
PCS statistics:									
RMSD [e]	0.26	0.20	1.30	1.27	0.98	0.48	0.45	0.35	-
MAD [e]	1.89	1.46	7.99	7.65	5.66	3.28	2.51	2.28	-
r_{xy} [e]	0.997	0.982	-0.795	-0.790	0.185	0.865	0.888	0.948	-
slope [e]	1.259	0.870	-0.341	-0.305	0.085	0.765	0.708	0.731	-

[a] χ-tensor calculated according to eq. (5) from the NEVPT2 *g*- and *D*-tensor given in Table S2 in SI. For measurement temperature 280 K. [b] Principal components of the traceless susceptibility tensor are sorted for best correspondence with the g_{ii} components (cf. SI). [c] In 10^{-32} m^3. [d] Euler angles φ, ϑ, ψ (in degree) in the ZX'Z' convention describing the χ-tensor orientation in the 5LAB frame (see SI). [e] RMSD (in ppm), maximum absolute deviation (MAD, in ppm), Pearson's correlation coefficient (r_{xy}), and slope of the correlation between calculated and "fitted experimental" PCSs (back-calculated from magnetic susceptibility tensors fitted to raw experimental PCSs[4a] with eq. (4), employing atomic positions from the newly refined X-ray structure 5LAB; see also Figure 3 and Figure S1).

The computed *g*- and *D*-tensors depend crucially on the input structure (Table S3 in SI), and this translates directly into the computed susceptibility tensors $\boldsymbol{\chi}$, and into the PCSs for the entire protein domain (Table 1 and Figure 3): the calculations for the original 1RMZ PDB structure provide too large susceptibility anisotropy parameters $\Delta\chi_{ax}$ and $\Delta\chi_{rh}$, while the χ-tensor orientation is nearly perfect. This is directly manifested in the corresponding PCS correlation plot (Figure 3), which shows an almost perfect correlation coefficient (excellent χ-tensor orientation), but a too large slope. DFT-optimized structures provide widely different quality of computed PCSs and χ-tensor. Several functionals provide no correlation whatsoever (Table 1, Figure S1 in SI), or even an anti-correlation (see, e.g., BP86-D3[12] structure in Figure 3) between computed and fitted experimental PCSs accompanied by reverse signs of the susceptibility anisotropy parameters $\Delta\chi_{ax}$ and $\Delta\chi_{rh}$. In contrast, the structure optimized at PBE0-D3 level[12c, 13] gives the best correlation with the fitted experimental PCSs among all DFT structures (although slightly inferior to the two X-ray structures, see also below; Table 1, Figure 3). This confirms the extreme dependence of PCSs on the local structure around the metal center.

We were intrigued by the overestimated slope of the PCS correlation plot for the 1RMZ structure (Figure 3, Table 1), which seemed to be too large to be explained by inaccuracies in the computed *g*- and *D*-tensors. Examination of the local coordination around the metal center showed that the X-ray data refinement had produced very unrealistic bond lengths within, as well as a non-planar configuration of, the NNGH hydroxamate inhibitor ligand,[7c] and also incorrect metal-ligand distances, in particular to NNGH. The non-planarity is not shared by any of the DFT-optimized model structures (cf. Table S1 in SI).

We therefore carried out a new refinement of the original X-ray data using REFMAC 5.8.0103 software.[14] The new structure differs from 1RMZ relatively little in the overall fold, but substantial changes occur around the NNGH inhibitor ligand, which now much better resembles the DFT-optimized structures (Figure 4, Table S1). The newly refined structure has been deposited at PDB under the access code 5LAB.

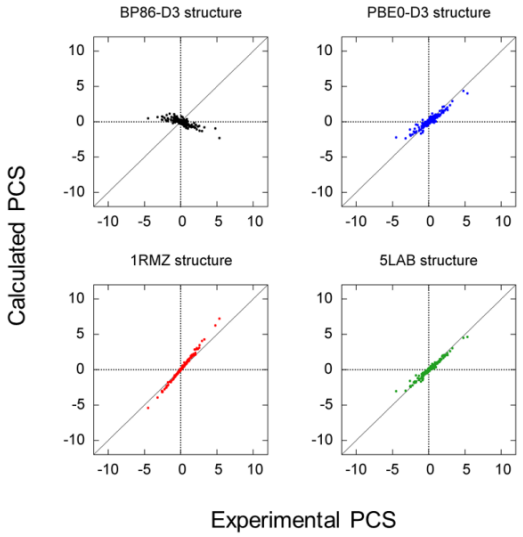

Figure 3. Selected correlations between quantum-chemically computed PCSs for different structures and fitted experimental data (obtained from magnetic susceptibility tensors fitted to raw experimental PCSs[4a]). All values are in ppm for 280 K. Further correlations are given in Figure S1 in SI.

Using it as a basis for our multi-scale computations, we obtain the PCS correlation plot with the best slope among all considered structures and still very good correlation (Table 1, Figure 3). That is, the orientation of the χ-tensor is coincidentally the best for the 1RMZ structure (albeit the structure around the metal center is flawed), but the magnitude of the computed tensor components is better for the 5LAB structure and not much inferior for the PBE0-D3 DFT-optimized structure. The structural variations affect the overall spin-density distribution (e.g., delocalization onto the NNGH ligand in Figure 4, Table S4, and Figure S2 in SI) only modestly, but sufficiently so to change the susceptibility anisotropy notably. Indeed, the large structure sensitivity of PCSs in such a metalloprotein may be used to judge the quality of structural models in great detail, and possibly to refine the local arrangement of the metal center, albeit the information content of

the susceptibility tensor χ (axial and rhombic components, as well as the three Euler angles, Table 1) is insufficient for a full structure optimization without taking into account further information from theory and/or experiment. We note also in passing that, ultimately, it will of course be desirable to include dynamical effects at suitable computational levels.

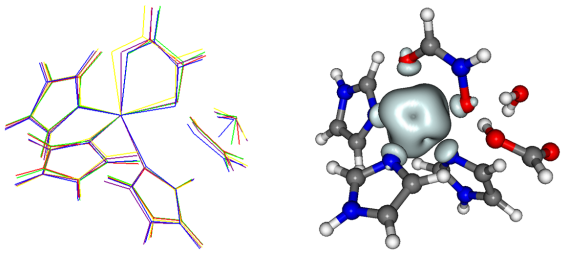

Figure 4. Left: comparison of the original 1RMZ metal coordination (red) with the newly refined 5LAB structure (green) and the structures optimized (within model *m1*) at the BP86 (yellow), PBE0 (purple), and PBE0-D3 (blue) levels. Right: spin-density distribution (PBE0-D3, 0.002 a.u. isosurface).

Importantly, however, calculations known to provide good prediction of the long-range PCSs should also provide detailed spectral assignment aids and electronic-structure information closer to the metal center, in a region in which experimental determination of the pNMR shifts is much more challenging. Full pNMR shifts for nuclei closer to the metal center are evaluated and compared to available experimental data[5] in Tables S5, S6, and Figure S3 in SI. While these comparisons expose shortcomings in DFT-computed HFCs, they nevertheless may be helpful for assignment and spectral-range predictions of signals, as we move closer into the "blind sphere" around the paramagnetic metal center.

In conclusion, hundreds of pseudo-contact shifts measured on a large paramagnetic metalloprotein can be accessed by a multi-scale quantum-chemical approach using accurate multi-reference wave-function methods, a point-dipole approximation, and modern pNMR shift theory, including the effects of zero-field splitting. The extreme dependence of computed pseudo-contact shifts on the coordination of the paramagnetic metal center represents a link between the local structure and the long-range experimental PCSs, and can provide information on the "blind sphere" of pNMR.

Acknowledgements

We thank Dr. Andrew J. Pell (Stockholm University) for useful discussions. This work has been carried out within the framework of the pNMR initial training network (Marie Curie Actions, EU Seventh Framework Programme, FP7/2007-2013, REA grant no. 317127). Further support by the UniCat Berlin DFG excellence cluster (for L.B. and M.K.) and the directed programme in Computational Science of the Academy of Finland (for J.M. and J.V.) is acknowledged. The work was also supported by Ente Cassa di Risparmio di Firenze, MIUR PRIN 2012SK7ASN, and CERM, part of the European Strategy Forum on Research Infrastructures (ESFRI). Computational resources from CSC – IT center for Science, Ltd. (Espoo, Finland) and TU Berlin are gratefully acknowledged.

Keywords: Ab initio calculations • Metalloproteins • NMR spectroscopy • Pseudo-contact shifts • Susceptibility tensor

[1] I. Bertini, C. Luchinat, G. Parigi, *Prog. Nucl. Magn. Reson. Spectrosc.* **2002**, *40*, 249-273.
[2] M. Allegrozzi, I. Bertini, M. B. L. Janik, Y.-M. Lee, G. Liu, C. Luchinat, *J. Am. Chem. Soc.* **2000**, *122*, 4154-4161.
[3] I. Bertini, C. Luchinat, G. Parigi, *Concepts Magn. Reson.* **2002**, *14*, 259-286.
[4] a) S. Balayssac, I. Bertini, A. Bhaumik, M. Lelli, C. Luchinat, *Proc. Natl. Acad. Sci. U. S. A.* **2008**, *105*, 17284-17289; b) I. Bertini, A. Bhaumik, G. De Paëpe, R. G. Griffin, M. Lelli, J. R. Lewandowski, C. Luchinat, *J. Am. Chem. Soc.* **2010**, *132*, 1032-1040; c) C. Luchinat, G. Parigi, E. Ravera, M. Rinaldelli, *J. Am. Chem. Soc.* **2012**, *134*, 5006-5009; d) M. J. Knight, I. C. Felli, R. Pierattelli, I. Bertini, L. Emsley, T. Herrmann, G. Pintacuda, *J. Am. Chem. Soc.* **2012**, *134*, 14730-14733; e) M. J. Knight, A. J. Pell, I. Bertini, I. C. Felli, L. Gonnelli, R. Pierattelli, T. Herrmann, L. Emsley, G. Pintacuda, *Proc. Natl. Acad. Sci. U. S. A.* **2012**, *109*, 11095-11100.
[5] I. Bertini, L. Emsley, M. Lelli, C. Luchinat, J. Mao, G. Pintacuda, *J. Am. Chem. Soc.* **2010**, *132*, 5558-5559.
[6] a) T. O. Pennanen, J. Vaara, *Phys. Rev. Lett.* **2008**, *100*, 133002; b) W. Van den Heuvel, A. Soncini, *J. Chem. Phys.* **2013**, *138*, 054113; c) S. A. Rouf, J. Mareš, J. Vaara, *J. Chem. Theory Comput.* **2015**, *11*, 1683-1691; d) J. Vaara, S. A. Rouf, J. Mareš, *J. Chem. Theory Comput.* **2015**, *11*, 4840-4849; e) B. Martin, J. Autschbach, *J. Chem. Phys.* **2015**, *142*, 054108; f) B. Martin, J. Autschbach, *Phys. Chem. Chem. Phys.* **2016**, *18*, 21051-21068.
[7] a) R. Lang, A. Kocourek, M. Braun, H. Tschesche, R. Huber, W. Bode, K. Maskos, *J. Mol. Biol.* **2001**, *312*, 731-742; b) I. Bertini, V. Calderone, M. Fragai, C. Luchinat, S. Mangani, B. Terni, *Angew. Chem. Int. Ed.* **2003**, *42*, 2673-2676; c) I. Bertini, V. Calderone, M. Cosenza, M. Fragai, Y.-M. Lee, C. Luchinat, S. Mangani, B. Terni, P. Turano, *Proc. Natl. Acad. Sci. U. S. A.* **2005**, *102*, 5334-5339.
[8] R. J. Kurland, B. R. McGarvey, *J. Magn. Reson.* **1970**, *2*, 286-301.
[9] J. Autschbach, S. Patchkovskii, B. Pritchard, *J. Chem. Theory Comput.* **2011**, *7*, 2175-2188.
[10] C. Angeli, S. Borini, M. Cestari, R. Cimiraglia, *J. Chem. Phys.* **2004**, *121*, 4043-4049.
[11] a) M. Sundararajan, D. Ganyushin, S. Ye, F. Neese, *Dalton Trans.* **2009**, 6021-6036; b) D. Maganas, S. Sottini, P. Kyritsis, E. J. J. Groenen, F. Neese, *Inorg. Chem.* **2011**, *50*, 8741-8754; c) R. Ruamps, L. J. Batchelor, R. Maurice, N. Gogoi, P. Jiménez-Lozano, N. Guihéry, C. de Graaf, A.-L. Barra, J.-P. Sutter , T. Mallah, *Chem. Eur. J.* **2013**, *19*, 950-956; d) M. Idešicová, J. Titiš, J. Krzystek, R. Boča, *Inorg. Chem.* **2013**, *52*, 9409-9417; e) R. Herchel, L. Váhovská, I. Potočňák, Z. Trávníček, *Inorg. Chem.* **2014**, *53*, 5896-5898; f) I. Nemec, R. Herchel, Z. Trávníček, *Sci. Rep.* **2015**, *5*, 10761; g) I. Nemec, R. Marx, R. Herchel, P. Neugebauer, J. van Slageren, Z. Trávníček, *Dalton Trans.* **2015**, *44*, 15014-15021; h) E. A. Suturina, D. Maganas, E. Bill, M. Atanasov, F. Neese, *Inorg. Chem.* **2015**, *54*, 9948-9961.
[12] a) A. Becke, *Phys. Rev. A* **1988**, *38*, 3098-3100; b) J. P. Perdew, *Phys. Rev. B* **1986**, *33*, 8822-8824; c) S. Grimme, J. Antony, S. Ehrlich, H. Krieg, *J. Chem. Phys.* **2010**, *132*, 154104.
[13] a) C. Adamo, V. Barone, *J. Chem. Phys.* **1999**, *110*, 6158-6170; b) J. P. Perdew, M. Ernzerhof, K. Burke, *J. Chem. Phys.* **1996**, *105*, 9982-9985.
[14] a) G. N. Murshudov, P. Skubak, A. A. Lebedev, N. S. Pannu, R. A. Steiner, R. A. Nicholls, M. D. Winn, F. Long, A. A. Vagin, *Acta Crystallogr. Sect. D* **2011**, *67*, 355-367; b) M. D. Winn, C. C. Ballard, K. D. Cowtan, E. J. Dodson, P. Emsley, P. R. Evans, R. M. Keegan, E. B. Krissinel, A. G. W. Leslie, A. McCoy, S. J. McNicholas, G. N. Murshudov, N. S. Pannu, E. A. Potterton, H. R. Powell, R. J. Read, A. Vagin, K. S. Wilson, *Acta Crystallogr. Sect. D* **2011**, *67*, 235-242.